Ab initio study of the physical properties of γ-Al_2O_3: Lattice dynamics, bulk properties, electronic structure, bonding, optical properties, and ELNES/XANES spectra

W. Y. Ching,[1,*] Lizhi Ouyang,[2,1] Paul Rulis,[1] and Hongzhi Yao[1]
[1]*Department of Physics, University of Missouri-Kansas City, Kansas City, Missouri 64110, USA*
[2]*Department of Physics and Mathematics, Tennessee State University, Nashville, Tennessee 37211, USA*
(Received 24 April 2008; revised manuscript received 10 June 2008; published 14 July 2008)

Based on the most recently determined noncubic structure for γ-Al_2O_3 by Menendez-Proupin and Gutierrez, a comprehensive list of physical properties is investigated theoretically. These include lattice dynamics and phonon spectra, elastic constants and bulk structural parameters, electronic structure and interatomic bonding, optical properties, and x-ray absorption near-edge structure (XANES) spectra. Compared to similar calculations of α-Al_2O_3, we find a smaller lowest zone-center vibrational mode at 97.6 cm^{-1}, a lower heat capacity, a smaller bulk modulus, and a much larger thermal-expansion coefficient. The threefold bonded O ions introduce highly localized vibrational modes near 751 cm^{-1}. The calculated thermal Grüneisen parameter indicates a strong anharmonicity in γ-Al_2O_3. The elastic tensor and the elastic wave velocities are also evaluated showing the longitudinal wave to be nearly isotropic. For the electronic structure, we find that γ-Al_2O_3 has a smaller band gap but a refractive index similar to α-Al_2O_3. Highly localized states at the top of the valence band originating from threefold bonded O in the more covalently bonded AlO_4 tetrahedra are identified. The calculated Mulliken effective charges and bond order values indicate that the structural model for γ-Al_2O_3 has a high degree of disorder. The octahedral unit (AlO_6) is a stronger polyhedron than the tetrahedral unit (AlO_4) although the latter has stronger Al–O bonds. The calculated Al-*K*, Al-L_3, and O-*K* edges for Al and O in γ-Al_2O_3 show strong dependence on their local coordination and environments. These results are in good agreement with available experimental data but the effect of the γ-Al_2O_3 samples' porosity should be properly assessed. It is argued that the traditional view that stoichiometric γ-Al_2O_3 is a defective spinel with cation vacancies (or its variations) should be modified. γ-Al_2O_3 is better described as an amorphous networklike structure such that the ratio of tetrahedrally coordinated Al to octahedrally coordinated Al is close to 0.6; and the O ions are bonded to Al in either a threefold or fourfold configurations in about equal proportion.

DOI: 10.1103/PhysRevB.78.014106 PACS number(s): 78.66.Nk, 63.20.dk, 71.23.−k, 78.70.Dm

I. INTRODUCTION

Alumina (Al_2O_3) is one of the most important structural ceramics with vast applications in a variety of industrial sectors ranging from pharmaceutical products and paint pigments to thermobarrier coatings and microelectronic devices, and much more.[1–4] Alumina exists in many different forms with corundum (α-Al_2O_3) being the most thermodynamically stable phase. The process of reaching α-Al_2O_3 involves many intermediate phases or the so-called transition aluminas (β-, γ-, η-, θ-, κ-, χ-, etc.).[5,6] Among these transition alumina, γ-Al_2O_3 is the most prominent and well studied because of its important application as a catalyst or catalytic support.[7–12] It also frequently occurs at ceramic interfaces or as a minor component in multiphase Al-containing ceramics such as in the Ca-Al-O and Al-Si-O systems.

In spite of many recent experimental[13–21] and theoretical[22–36] studies of γ-Al_2O_3, there are continuing debates about its structure and properties. γ-Al_2O_3 does not exist in the pure single-crystal form. The samples obtained are usually porous with large surface areas. The traditional view of the structure of γ-Al_2O_3 is that of a defective cubic spinel with cation vacancies,[37] or the spinel lattice model. In the spinel lattice AB_2O_4, where A is the tetrahedral cation site and B the octahedral cation site, vacancies are required at the cation sites in order to fit the exact stoichiometric formula of Al_2O_3. There were then debates as to whether the vacancy should occur at the A site or the B site or both.[22–24,26] The issue of the presence of H in γ-Al_2O_3 has also been raised. However, it has been ruled out by extensive simulation on spinel based models.[25] The spinel lattice model has been challenged recently[28,32,34,35] and models with tetragonal[28] and monoclinc[35] structures have been suggested. Very recently, it is noted that the spinel model was still being defended on the basis of x-ray powder-diffraction patterns,[36] but this argument was soundly refuted as due to problems with the samples.[38,39] The common underlying message is that Al occupies both the octahedral and tetrahedral sites in the lattice. Recently, more rigorous theoretical simulations suggest that that structure of γ-Al_2O_3 is not a spinel with cation vacancy, but is instead a low-symmetry crystal structure with a space group of $I4_1/amd$ in which Al ions can have both tetrahedral and octahedral coordination.[30] In this structure, the notion of ionic vacancy becomes less clear and an alternative description in terms of local bonding is more appropriate. Unlike α-Al_2O_3 with a rhombohedral lattice, where O ions are always fourfold bonded, the O ions in γ-Al_2O_3 can be either threefold or fourfold bonded, a fact shared by many other transition alumina such as θ-Al_2O_3 and η-Al_2O_3,[6,40] but seldom discussed. Thus, a proper description of the structure of γ-Al_2O_3 should include the ratios of Al_{tet}/Al_{oct} and $O_{3\text{-fold}}/O_{4\text{-fold}}$. As a matter of fact, it is conceivable that amorphous Al_2O_3 (a-Al_2O_3) can be viewed as a continuous random network with a variety of total Al and O local bonding environments connected in a random fashion.[41] The specific local cation/anion coordination pro-

TABLE I. Crystal structure and calculated physical properties of γ-Al_2O_3 and α-Al_2O_3.

	γ-Al_2O_3	α-Al_2O_3
Space group	$I4_1/amd$ (NO 141) P1	R-3c (NO 167)
Lattice parameters:		
a, b, c (Å)	5.6061, 5.5699, 13.4820	$a=b=c=5.128$
α, β, γ	89.4° 90.0° 120.0°	$\alpha=\beta=\gamma=55.3318°$
# Atoms/cell	40	10
	Al_{tet}: 6, Al_{oct}: 10	Al_{tet}: 4
	$O_{3\text{-fold}}$: 12, $O_{4\text{-fold}}$: 12	$O_{4\text{-fold}}$: 6
Band gap (eV)	4.22	6.33
Upper VB width (eV)	8.8	7.20
Lower VB width (eV)	4.0	3.60
$\varepsilon_1(0)$, n	3.153, 1.776	3.1413, 1.772
$\varepsilon_1(\hbar\omega$ at 590 nm=2.10 eV), n	3.233, 1.799	3.2035, 1.790
Experimental n	-	1.769
ω_p (eV)	20.5	21.1
Average Q^*	Al_{tet}: 1.46 Al_{oct}: 1.58	Al_{oct}: 1.557
	$O_{3\text{-fold}}$: 6.99 $O_{4\text{-fold}}$:6.96	$O_{4\text{-fold}}$: 6.962

vides the short-range order of the network, but the long-range order is absent as in any other typical inorganic glass.

Although the importance of γ-Al_2O_3 and its many applications have been well recognized by the research community, there is little experimental data on pure samples of γ-Al_2O_3. Work has been reported on structure determination using x-ray diffraction (XRD) [Ref. 6] and transmission electron microscopy (TEM).[18,37] Infrared (IR) spectroscopy,[14,20] x-ray emission spectroscopy,[13] x-ray photoelectron spectroscopy,[19] and Al NMR spectroscopy[20,21,23] have been used to study γ-Al_2O_3 films or related materials. Electron energy-loss spectroscopy (EELS) has played a very important role in the characterization of γ-Al_2O_3.[15–17] However, most of these measurements are either inclusive of surface effects, on porous samples, or with intentionally doped transition-metal elements as part of the sample preparing process. Without a clear understanding of the properties of pure bulk γ-Al_2O_3, interpretation of these experimental data will be difficult or even misleading. In this respect, careful *ab initio* calculations on a well defined structural model of γ-Al_2O_3 can provide much of the missing information that can be used to properly interpret the data for more complex and nonstoichiometric samples.

In this paper, we report a comprehensive study of many of the physical properties of γ-Al_2O_3 based on the structure published in Ref. 26. The crystal structure reported by these authors is far superior to other models proposed earlier and could represent the smallest unit cell of the true bulk γ-Al_2O_3 that contains all the essential ingredients of the structure of γ-Al_2O_3. We used their data as the initial structure and further relaxed the atomic positions with high accuracy using the VIENNA *Ab initio* SIMULATION PACKAGE (VASP).[42,43] A high energy cutoff of 600 eV and a $5\times5\times2$ Monkhorst k-point sampling were used. The criteria for electronic state updating and ionic step updating were set to 10^{-7} eV and 10^{-4} eV/Å, respectively. The structure we obtained does not change significantly from that in Ref. 26. The structural information of this model is listed in Table I together with that of α-Al_2O_3. It should be pointed out that due to atomic relaxation, all atoms in the unit cell are crystallographically nonequivalent and the structure is more likely to have a space group of P1. The unit cell of this model contains 40 atoms, 16 Al (6 Al_{tet} and 10 Al_{oct}) and 24 O (12 $O_{3\text{-fold}}$ and 12 $O_{4\text{-fold}}$) so the cation percentage for Al_{tet} (Al_{oct}) is 37.5% (62.5%). Likewise, the anion percentage for $O_{3\text{-fold}}$ and $O_{4\text{-fold}}$ are both 50%. The reported experimental NMR data indicated a smaller percentage of the Al_{tet}.[20,21,23] However, the samples used in these studies were all derived at high temperature with a large percentage of surface area, and its structure can be significantly different from the bulk crystalline model used in the present study. Figure 1 shows the crystal structure model of γ-Al_2O_3 with distinguishing marks for the different types of ions and polyhedra. For comparison, in the spinel lattice the tetrahedral site and octahedral site percentages are 33.3%, and 66.7%, respectively. This implies that there are more tetrahedral sites than octahedral sites in the present model compared to the ideal spinel lat-

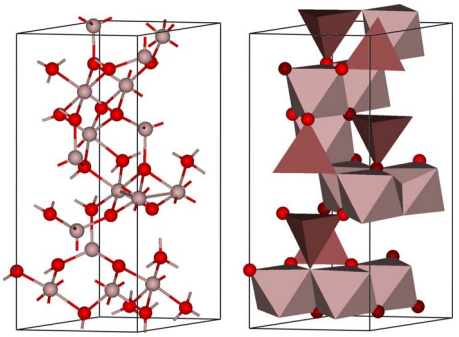

FIG. 1. (Color online) Ball and stick model of γ-Al_2O_3. The pink (red) balls are for Al (o); (b) Same model showing the polyhedra with a dark shade for Al_{tet} and a light shade for Al_{oct}.

tice, or equivalently, cation vacancies should be at the octahedral site if the spinel lattice model for γ-Al_2O_3 is adopted. This is consistent with an earlier investigation[22] and with a number of other studies.[24,26] In the spinel lattice, all O are fourfold bonded. The creation of cation vacancies naturally leads to threefold bonded O. The distribution of O coordination in γ-Al_2O_3 has not been discussed in the past. In most oxides, the likely O coordination is either twofold (bridging) such as in quartz, or fourfold as in α-Al_2O_3. It may assume sixfold coordination in some high-pressure phases such as in stishovite. The threefold coordinated O is a special feature in most transition alumina. The electronic structure and spectroscopic properties of crystals with threefold coordinated O can be very different from those with twofold or fourfold coordination.[40,44,45]

Our calculations of the physical properties of γ-Al_2O_3 using the above structure includes lattice dynamics and phonon spectra, temperature-dependent thermodynamic functions, vibrational contribution to the free energy, bulk elastic parameters and elastic wave velocities, electronic structure and bonding, interband optical properties, and x-ray absorption near-edge structure (XANES) spectra for Al and O with different local coordinations. In principle, the XANES spectra are similar to the electron energy-loss near-edge spectroscopy (ELNES) spectra and there are some limited experimental XANES/ELNES measurements for γ-Al_2O_3.[15–17] We are not aware of any previous calculations of the phonon spectrum of γ-Al_2O_3 using a fully *ab initio* method. Lodiana and Parlinski did the phonon calculations for α-Al_2O_3 and θ-Al_2O_3(Ref. 46) but not γ-Al_2O_3. Very recently, Lee *et al.*[33] carried out electronic structure and dielectric properties calculations of four alumina polymorphs including γ-Al_2O_3. They have also calculated the zone-center phonons in these polymorphs. However, the structure they used for γ-Al_2O_3 is an earlier model structure,[26] different from the one we used in the present calculation. Our results will be compared with available experimental data and other existing calculations whenever possible.

The paper is organized as follows. In Sec II, we describe our calculations of the vibrational properties and present our results on the thermodynamic functions of γ-Al_2O_3. In Sec III, we present the elastic properties and bulk structural parameters for γ-Al_2O_3 and compare them to α-Al_2O_3. In Sec IV, we discuss the results of the electronic structure and bonding calculated using the orthogonalized linear combination of atomic orbitals method (OLCAO).[47] The spectroscopic properties which include the valence-band optical properties and the Al-*K*, Al-L_3 and O-*K* edges of the XANES are presented and discussed in Sec V. We further discuss these results and their implications in Sec VI together with a brief summary.

II. LATTICE DYNAMICS AND THERMO PROPERTIES

In recent years, it has become possible to calculate the lattice dynamic properties of crystals based on fundamental *ab initio* electronic structures.[48] The lattice dynamics of γ-Al_2O_3 were studied within the qausiharmonic approximation (QHA) by calculating the phonon spectrum using a first-principles approach. The VASP code in conjunction with an in-house package GPT [stands for $G(P,T)$] were used. A $2\times2\times1$ supercell was used for the phonon calculation of γ-Al_2O_3. The calculation is very demanding because the equilibrium structure must be highly accurate and, since the 160 atom supercell has no internal symmetry to reduce the computational burden, the interatomic forces for the displacement of every atom must be explicitly computed. In the present calculation, we used: (1) ultrasoft pseudopotentials with Ceperley-Alder approximation for exchange-correlation;[49] (2) a single Γ k point for structure optimization and phonon calculation for the supercell which is sufficient since the volume of the supercell is kept fixed; (3) "accurate" accuracy for the VASP calculations with an energy cutoff of 400eV; (4) energy and force convergence criteria of 1.0×10^{-5} eV and 0.001 eV/Å, respectively; (5) a $20\times20\times20$ k-space mesh for Brillouin-zone (BZ) integration of the phonon density of state (DOS). The phonon density of states $g(\omega)$ and the site specific partial density of states (PDOS) $g_\alpha(\omega)$ are evaluated according to,

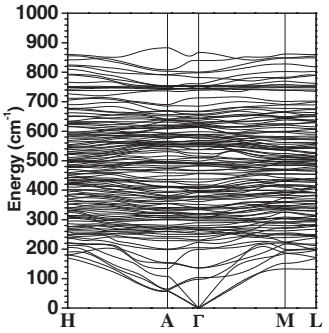

FIG. 2. Calculated phonon-dispersion spectrum of γ-Al_2O_3.

$$g(\omega)=\frac{1}{n}\sum_{q,i}\delta[\omega-\omega_i(\vec{q})]$$

$$g_\alpha(\omega)=\frac{1}{n}\sum_{\vec{q},i,\mu}|e^i_{\alpha,\mu}(\vec{q})|^2\delta[\omega-\omega_i(\vec{q})] \quad (1)$$

where ω_i is the phonon frequency, n is the number of q points, q and i are wave vector and phonon branch indices, δ is the thermal broadening function and $e^i_{\alpha,\mu}(\vec{q})$ is the polarization vector of the α^{th} atom along the μ^{th} direction for the i^{th} branch phonon at wave vector q. In the present calculation, we did not include the correction for the longitudinal optical (LO) and transverse optical (TO) splitting which requires calculation of the optical dielectric constant and Born effective charges of each nonequivalent atom using the Berry phase method.[50] We do not expect it to have a large effect in the present study for γ-Al_2O_3.

Figure 2 shows the calculated phonon-dispersion curves along the high-symmetry directions of the BZ. For a better comparison with corundum, we approximated the BZ to be that of a hexagonal lattice since in the present model for γ-Al_2O_3 ($a\sim b$, α and $\beta\sim90°$, and $\gamma\sim120°$), see Table I for more details. The 40 atom cell gives a total of 120 branches with the maximum frequency just shy of 900 cm^{-1}. The cor-

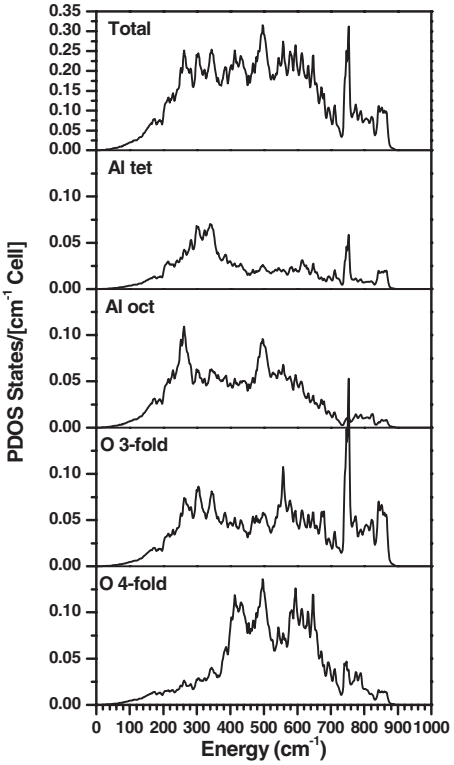

FIG. 3. Calculated vibrational DOS and partial DOS of γ-Al_2O_3. (a) Total, (b) Al_{tet}, (c) Al_{oct} (d) $O_{3\text{-fold}}$, and (e) $O_{4\text{-fold}}$.

responding phonon DOS and partial DOS are shown in Fig. 3. The notable Von Hove peak at the high frequency of 750 cm^{-1} is due to "breathing"-like Al–O bond stretching of the tetrahedral AlO_4 unit, which is notably higher than corresponding modes in corundum.[46] This can be explained by the shorter Al–O bond distance of about 1.73 Å found in the present model. The Von Hove peak near 500 cm^{-1} is due to the breathing mode of the octahedral AlO_6 unit. The overall DOS of γ-Al_2O_3 resembles that calculated for κ-Al_2O_3 using first-principles methods.[33] There is notable broadening of the few localized modes in comparison to corundum. The broadening of these localized modes and the reduction of some more diffusive peaks reflects the disruption of longer range order while maintaining short-range order in the γ-Al_2O_3 model. This may be viewed as a signature of an amorphouslike structure.

The zone-center vibrational modes give information on the Raman and IR active modes in a solid. Because of the reduced symmetry, symmetry analysis for these modes in γ-Al_2O_3 will not be informative. Instead, we plot the zone-center mode frequencies as a histogram in Fig. 4 with a small window of 5 cm^{-1}. According to the calculation, the four lowest frequencies are at 97.6, 103.8, 136.0, and 136.4 cm^{-1}. The highest frequency mode is at 870.8 cm^{-1}. A peak at 750 cm^{-1} is also present which contributes to the peak in the DOS of Fig. 3.

From the phonon spectrum of γ-Al_2O_3 at different volumes V (see below), we can obtain the mode-Grüneisen parameter for each phonon branch defined as:

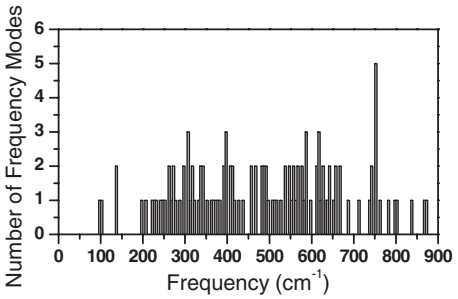

FIG. 4. Distribution of frequency modes at the Γ point for γ-Al_2O_3.

$$\gamma_i(q) = -\partial\{\ln \omega_i(q)\}/\partial\{\ln V\}. \tag{2}$$

The Grüneisen parameter is often used to characterize frequency changes under applied strain. We found that most mode-Grüneisen parameters are positive and dispersed around 1.0 similar to those of corundum.[51] However, the lowest optical mode gives a negative mode-Grüneisen parameter of −0.20, a feature found in many bulk amorphous materials.[52–54]

We now proceed to the calculation of Gibb's free energy $G(P,T)$ or $G(V,T)$ for γ-Al_2O_3. Once the phonon spectrum is calculated, it is possible to estimate all other thermodynamic functions.[48] Within the Born-Oppenheimer approximation, the Helmholtz free energy of a solid can be decomposed into two parts:

$$F(V,T) = F^{\text{el}}(V,T) + F^{\text{vib}}(V,T), \tag{3}$$

where V is the volume of the unit cell, T is the temperature, $F^{\text{el}}(V,T)$ and $F^{\text{vib}}(V,T)$ are free-energy contributions due to electron motion and nuclear vibration, respectively. For insulators at ambient temperature, the thermal excitation energy and entropy contribution to electron free energy $F^{\text{el}}(V,T)$ are negligible, and we may write:

$$F^{\text{el}}(V,T) = U^{\text{el}}(V,T) - TS^{\text{el}}(V,T) \approx U^{\text{el}}(V,0) = E^{\text{el}}(V), \tag{4}$$

where $E^{\text{el}}(V)$ is the ground-state total energy for the electrons within the framework of density-functional theory. Within the QHA, the nuclear vibrational free energy is given by,

$$F^{\text{vib}}(V,T) = \sum_{q}^{BZ} \sum_{i}^{3N} \left\{ \tfrac{1}{2}\hbar\omega_i(V,\vec{q}) + k_B T \ln(1 - e^{-\hbar\omega_i(V,\vec{q})/k_B T}) \right\} \tag{5}$$

where the first term in the summation is the zero-point energy, q is a wave vector in the BZ, i is the phonon branch index, $\omega_i(V,q)$ is the phonon frequency of the i^{th} branch at wave vector q for volume V. The vibrational entropy $S^{\text{vib}}(V,T)$ can be calculated according to,

$$S^{\text{vib}}(V,T) = \sum_{\vec{q}}^{BZ} \sum_{i}^{3N} \left\{ k_B \ln(1 - e^{-\hbar\omega_i(V,\vec{q})/k_BT}) + \frac{\hbar\omega_i(V,\vec{q})}{T} \frac{e^{-\hbar\omega_i(V,\vec{q})/k_BT}}{1 - e^{-\hbar\omega_i(V,\vec{q})/k_BT}} \right\}. \quad (6)$$

From the Helmholtz free energy $F(V,T)$, we can now evaluate the Gibbs free energy $G(P,T)$ and enthalpy $H(P,T)$,

$$G(P,T) = F(V,T) + PV, \quad H(P,T) = G(P,T) + TS, \quad (7)$$

where

$$P(V,T) = -(\partial F/\partial V)_T \quad (8)$$

and S is the vibrational part of the entropy. The specific procedures used in the GPT package to calculate the Gibbs free energy $G(P,T)$ are outlined as follows: (1) A series of phonon calculations are performed at different volumes; typically, deviating from the ground-state volume by −3% to 3% at 1% increments. For each volume, the crystal structure is fully optimized allowing both crystal shape and internal coordinates to be adjusted. $F(V,T)$ is then calculated for that volume. (2) The pressure $P(V,T)$ is calculated based on Eq. (8). At a given temperature T, the Helmholtz free energy $F(V,T)$ is fitted into a fourth order polynomial function of the volume V. The fitting process is carefully monitored as it may indicate that either higher accuracy in the phonon calculation is desirable or more phonon calculations at different volumes are needed. The obtained polynomial function is then used to calculate Holmholtz free energy $F(V,T)$ at a given P and V. (3) The Gibbs free energy $G(P,T)$ and enthalpy H are calculated using the obtained $P(V,T)$ in the previous step. We first obtain volume V for given pressure P and temperature T and then calculate Gibbs free energy and enthalpy using Eq. (7).

From the above obtained Helmholtz free energy $F(V,T)$, entropy $S(V,T)$, pressure $P(V,T)$, and Gibbs free energy $G(P,T)$, it is straightforward to calculate other important thermodynamic properties. These include the constant volume specific heat $C_v = T(\partial S/\partial T)_V$, volume thermal-expansion coefficient $\alpha_V(T) = d\{\ln V(T)\}/dT$, isothermal bulk modulus $B(T) = -1/\{d[\ln V(T)]/dP\}$, thermal Grüneisen parameter $\gamma_{\text{th}} = [V\alpha_V(T)B(T)/C_V]$, and constant pressure specific heat $C_P = [1 + \gamma_{\text{th}}\alpha_V(T)]C_V$. Figures 5 and 6 summarize some of the calculated temperature-dependent thermodynamic functions for γ-Al_2O_3 discussed above. At ambient conditions of P and $T = 295$ K, the volume thermal-expansion coefficient, volume specific heat, isothermal bulk modulus, thermal Grüneisen parameter, and constant pressure specific heat are found to be 13.62×10^{-6} K^{-1}, 794 J/K kg, 195.66 GPa, 0.910, and 794 J/K kg, respectively. Compared to the corresponding values for corundum (16×10^{-6} K^{-1}, 775 J/K kg, 255 GPa, 1.30, and 775 J/K kg),[55] γ-Al_2O_3 has a slightly larger heat capacity and smaller bulk modulus, thermal-expansion coefficient and thermal Grüneisen parameter.

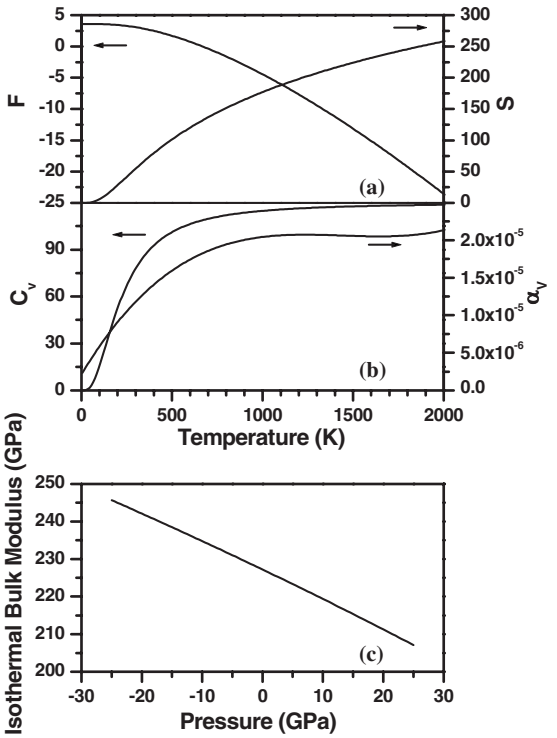

FIG. 5. Temperature dependent thermodynamic properties: (a) F vs T; S vs T; (b) C_v vs T; α_V (10^{-6} K^{-1}) vs T; (c) Isothermal bulk modulus at 295 K as a function of P.

III. STRUCTURAL PROPERTIES

Most of the structure properties of a crystal can be easily derived from its elastic constants. The elastic constants of γ-Al_2O_3 are calculated using the VASP optimized structure and the elastic tensor module included in the GPT package that was designed for efficient evaluation of the stress-strain response. Details about the method have been described in a recent paper.[56] In the actual calculation for γ-Al_2O_3, seven strain levels ε_j ranging from −1% to 1% were applied to each independent deformation and the stress data σ_i were collected from the fully *ab initio* calculations. The elastic constants C_{ij} were then extracted by solving the system of linear equations, $\sigma_i = \Sigma_{j=1}^{6} C_{ij}\varepsilon_j$. The resultant elastic constants C_{ij} for γ-Al_2O_3 are listed in Table II. Note that for the upright off-diagonal 3×3 matrix in the elastic tensor, only C_{14}, C_{24}, and C_{34} are nonzero. Apparently, the elastic tensor of γ-Al_2O_3 in the present structure shows the symmetry of a monoclinic crystal lattice with a twofold-symmetry axis in the x direction or a mirror plane perpendicular to the x axis.[57]

From the calculated elastic constants of a single crystal, it is possible to extract the bulk structure parameters K (bulk modulus), G (shear modulus), E (Young's modulus) and η (Poisson's ratio) of polycrystalline γ-Al_2O_3. Although there are different ways of getting the bulk structural parameters, the scheme we used is the Voigt-Reuss-Hill (VRH) approximation which averages anisotropic elastic properties of the single crystal to obtain isotropic properties of the corresponding polycrystals.[58–60] The calculated elastic constants and bulk parameters using the VRH scheme are listed in Table III together with that of α-Al_2O_3 for comparison. To

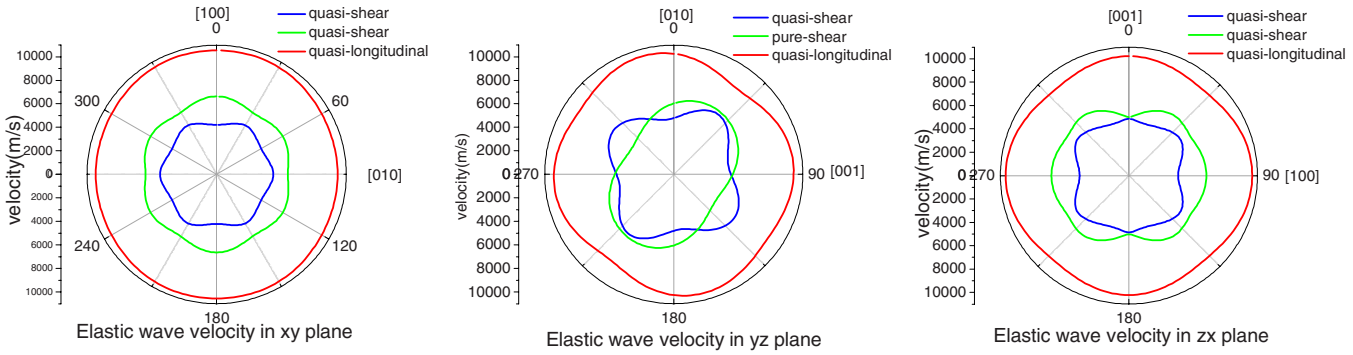

FIG. 6. (Color online) Plots of sound velocity in a plane. (a) *x*-*y* plane velocity plot shows the sixfold symmetry in two quasishear modes. (b) *y*-*z* plane velocity plot has twofold symmetry in both the longitudinal and transverse modes. One shear wave mode is pure. (c) *z*-*x* plane velocity plot has a twofold symmetry in both modes. There is no pure mode in the plane.

our knowledge, this is the first time such data were calculated for γ-Al_2O_3 based on whatever structures were assumed. In general, γ-Al_2O_3 has smaller elastic constants than α-Al_2O_3 except for C_{14} where γ-Al_2O_3 is significantly larger by almost 80% (34.9 GPa vs 19.4 GPa). γ-Al_2O_3 also has a slightly larger Poisson's ratio which indicates that it is less compressible. The calculated bulk modulus for γ-Al_2O_3 is 204 GPa, larger than the value of 175 GPa reported in Ref. 35 and smaller than the value of 219 GPa of Ref. 26. Obviously, the difference comes from the different structural models used for γ-Al_2O_3. We are not aware of any experimental bulk modulus for γ-Al_2O_3. Even if it is available, it could be somewhat smaller than the theoretical values because of the thin-film or porous nature of the samples.

From the elastic tensor, we can compute the elastic wave velocity along specific directions by solving the Christoffel wave equationm,[61]

$$\rho v^2 u_i = C_{ijkl} l_j l_k u_l. \tag{9}$$

In Eq. (9), ρ is the density, v is the elastic wave velocity, C is the elastic tensor, l is the direction of the k vector, and u_i is the polarization of the elastic wave. Figure 6 displays the inverse sound velocity of the three acoustic modes along all directions in the *x*-*y*, *y*-*z*, and *z*-*x* planes. The longitudinal high-frequency mode is nearly spherical, indicating that the longitudinal wave is isotropic in the *x*-*y* plane. The two transverse modes, however, show a sixfold symmetry which is a feature of a crystal lattice with a threefold symmetry, i.e., the trigonal lattice. We note that the anisotropy is significant only for the transverse modes. For longitudinal waves, the γ-Al_2O_3 behaves like a homogenous media. This may indicate that some crystalline features remain in the present γ-Al_2O_3 model.

IV. ELECTRONIC STRUCTURE AND BONDING

The electronic structure and bonding in γ-Al_2O_3 is studied using the first-principles OLCAO method.[47] Over the years, we have been using this DFT-based method in its local approximation (LDA) for electronic structure and optical properties calculations of many crystals and complex microstructures with great success.[47,62–73] The method has been amply described in published papers and should not be repeated here. In the present study, we used the atomic orbitals of Al $(1s,2s,3s,4s,5s,2p,3p,4p,5p,3d,4d)$ and O $(1s,2s,3s,4s,2p,3p,4p)$ for a full basis expansion. A large number of k points (864) in the irreducible portion of the BZ are employed in the BZ integration.

The calculated band structure and total DOS are show in Figs. 7 and 8, respectively. For convenience, we used the notation of a hexagonal lattice to label the symmetry points and axes. The calculated band structure for γ-Al_2O_3 is almost identical to that of Ref. 30 using a different method. γ-Al_2O_3 is an insulator with a sizable LDA gap of 4.22 eV. The real gap could be 30%–35% larger to account for the deficiency of the LDA theory. The top of the valence band (VB) is rather flat from A to Γ and the bottom of the conduction band (CB) is at Γ and consists of a single band. As indicated in Fig. 1, we classify the atoms in γ-Al_2O_3 as Al_{tet}, Al_{oct}, $O_{3\text{-fold}}$, and $O_{4\text{-fold}}$ on the basis of their local coordina-

TABLE II. Elastic tensor of γ-Al_2O_3.

C_{ij}	1	2	3	4	5	6
1	4162.5	1272.3	979.3	348.5	0	0
2	1272.3	3908.5	1005	−305.8	−0.3	0
3	979.3	1005	3902.5	75.8	0	0
4	348.5	−305.8	75.8	892.5	0	−0.3
5	0	−0.3	0	0	942.5	442.0
6	0	0	0	−0.3	442	1365.0

TABLE III. Calculated elastic constants and bulk structural parameters of γ-Al_2O_3 and α-Al_2O_3 in unit of GPa.

Crystals	C11	C12	C13	C14	C33	C44	C66	K	G	E	η
γ-Al_2O_3	416.3	127.2	97.9	34.9	390.3	89.3	136.5	204.0	113.2	286.5	0.266
α-Al_2O_3	476.8	157.4	119.4	19.4	-	145.5	-	246.9	158.5	391.6	0.237

tion. The partial DOS (PDOS) for the two types of Al and two types of O are shown in Fig. 8. It can be seen that there are enormous differences between the PDOS of Al_{tet} and Al_{oct}, and also between $O_{3\text{-fold}}$ and $O_{4\text{-fold}}$. For Al, the main differences are in the CB whereas for O, the differences are mostly in the VB region. Al_{tet} has a huge peak at 7.3 eV in the lower CB region and another peak at 13.7 eV. From orbital-resolved PDOS (not shown), it is revealed that the lower peak involves strong hybridization of Al-*p* and Al-3*d* orbitals whereas the higher peak predominately originates from the 3d orbitals. The Al_{oct} has a completely different CB DOS, featuring two main peaks at 11.5 and 13.7 eV. The orbital origins of these peaks are states dominated by Al-3*d* and Al-4*p* orbitals, respectively. These different features in the CB DOS are also reflected in the different XANES/ELNES spectra to be discussed in Sec. V.

The PDOS for the O can be clearly divided into two segments, the upper 2*p* band (0 to −8.8 eV) and the lower 2*s* band (−16.4 to −20.4 eV). The spectral weights of the $O_{3\text{-fold}}$ and $O_{4\text{-fold}}$ in these two regions and their peak positions are different. By having one more bond, $O_{4\text{-fold}}$ has peaks in the PDOS at a lower binding energy than does $O_{3\text{-fold}}$, so, the O-2*s* peaks are centered at −18.5 and −17.1 eV, respectively. The top of the VB is derived mostly from the 2*p* states of $O_{3\text{-fold}}$. The peak structures and their binding energies can be easily revealed by x-ray photoelectron (XPS) or soft x-ray emission spectroscopy. However, it takes theoretical results to resolve them into partial components of atoms with different local coordination. The VB DOS is in good agreement with the XPS data of Ealet *et al.*[19] Our calculated DOS and PDOS have minor deviations from that of Digne *et al.*[35] which can be attributed to the difference in the structural models used for γ-Al_2O_3.

Figure 9 shows the localization index L_n of each electron state *n* across the energy range according to:

$$L_n = \sum_{i,\alpha} \left[\sum_{j,\beta} C_{i\alpha}^{*n} C_{j\beta}^{n} \right]^2, \qquad (9')$$

where $C_{i\alpha}^{n}$ are the eigenvector coefficients for the n^{th} state with orbital and atomic specifications of *i* and α. Each data point is the average of the states over all *k* points in the BZ. L_n is used mostly to characterize electron states of amorphous systems using large structural models.[74–76] For a noncrystalline solid, the states near the band edges are usually more localized. It is interesting to note that even with only 40 atoms in the cell, the L_n shows the states at the top of the VB to be highly localized, indicating that γ-Al_2O_3 resembles more of an amorphous glass than an inorganic crystal. Inspection of the wave functions (also from the PDOS of Fig. 8) reveals that the two highly localized states at the top of the VB originate from two of the 12 $O_{3\text{-fold}}$ atoms (labeled with atom number 19 and 21). What makes these two $O_{3\text{-fold}}$ atoms different from the others such that they are responsible for the highly localized electron states at the top of the VB? We found that these two atoms experience the least significant charge transfer from Al, or that they have a more covalent character to their bonding (see Fig. 10). These two atoms are also the only $O_{3\text{-fold}}$ atoms in the tetrahedral units that contain only one $O_{3\text{-fold}}$ ion, and they have a total bond order

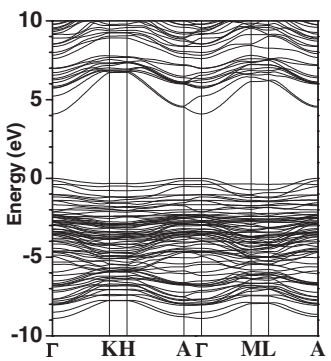

FIG. 7. Calculated band structure of γ-Al_2O_3.

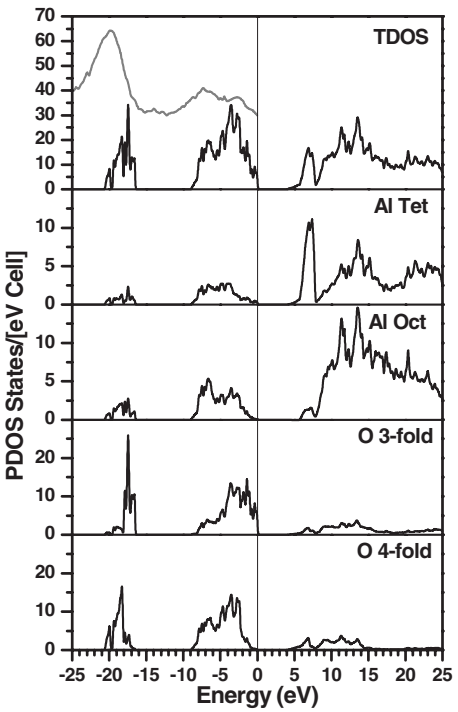

FIG. 8. Calculated total and partial DOS of the electron states in γ-Al_2O_3.

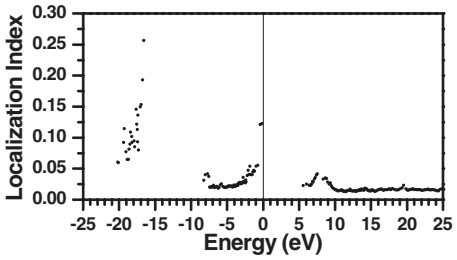

FIG. 9. Calculated localization index L_n for the k-averaged electron states of γ-Al_2O_3.

value that is ~0.2 greater than the other tetrahedral units (see discussion below). This indicates that these two $O_{3\text{-fold}}$ atoms have particularly strong bonds within the specific AlO_4 tetrahedral units. These are the same $O_{3\text{-fold}}$ ions that give the strong vibrational peak at 750 cm^{-1} discussed in Sec II.

The Mulliken effective charges Q^* on each atom and the bond order (BO) (or the overlap population) between pairs of ions in a crystal are very useful quantities to describe interatomic bonding and charge transfer. They are calculated separately using a minimal basis set. In the OLCAO method where the wave functions are expanded in terms of localized atomic orbitals, the application of the Mulliken population analysis[77] to obtain Q^* and BO is both convenient and natural since it involves no artificial choice of atomic radii for different types of atoms. In some other electronic structure methods where plane-wave basis sets are used for expansion, the Bloch functions need to be projected onto atomic spheres of a given radius. Such procedures introduce some uncertainty since there is no specific criterion as to what radius should be used for Al_{tet} and Al_{oct}, or for $O_{3\text{-fold}}$ and $O_{4\text{-fold}}$. Figure 10 displays the calculated Q^* of the 40 atoms (Al and O) in γ-Al_2O_3. Figure 11 shows the distribution of the calculated BO values and the bond lengths between different Al-O pairs. These results can be succinctly summarized as

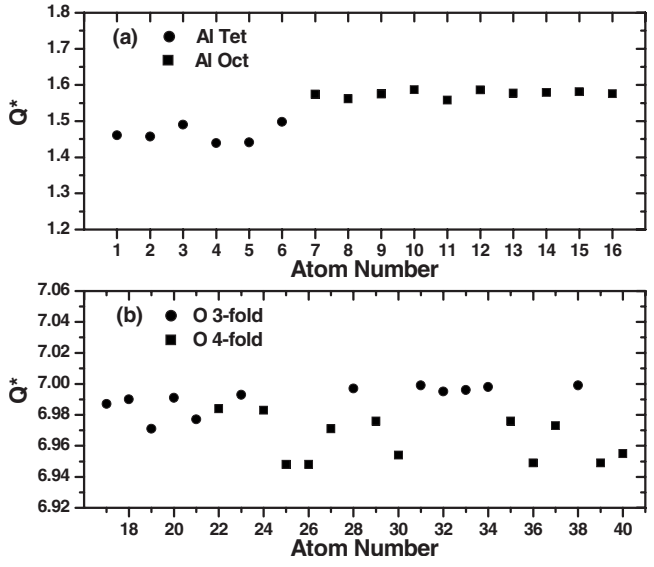

FIG. 10. Calculated Mulliken effective charges Q^* of (a) Al ions (Circle: Al_{tet}; Square: Al_{oct}); (b) O ions. (Circle: $O_{3\text{-fold}}$; Square: $O_{4\text{-fold}}$).

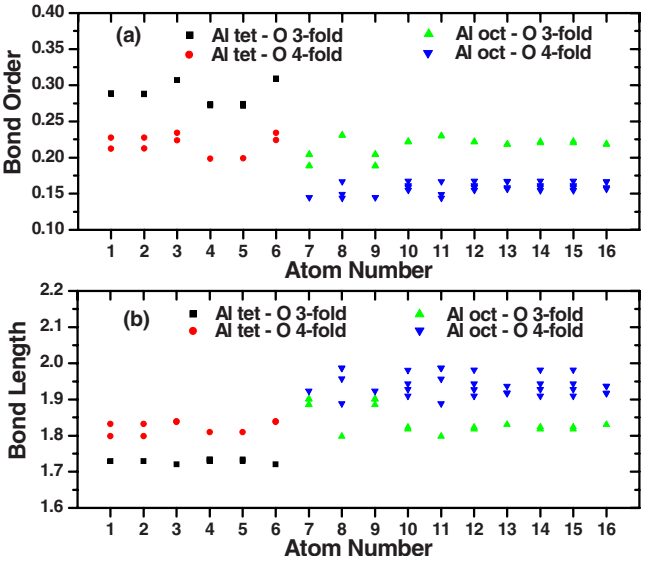

FIG. 11. (Color online) Distribution of: (a) calculated Al-O bond order values and (b) Al-O bond lengths in γ-Al_2O_3.

follows: (1) Q^* is lower in Al_{tet} compared to Al_{oct} with average values of 1.46 and 1.58 electrons, respectively; (2) The Q^* for Al_{oct} is fairly constant whereas Al_{tet} has larger variations; (3) the Q^* for $O_{3\text{-fold}}$ are slightly larger than for $O_{4\text{-fold}}$ with average values of 6.99 and 6.96, respectively. There are variations within each group. (4) The Al–O bond lengths show two distinct values for Al_{tet}, while for Al_{oct} they have either two or three distinct values. The corresponding BO values scale approximately inversely with the bond length. (5) The BO values for Al_{tet}-O are higher than those of Al_{oct}-O, indicating a stronger individual Al–O bond in the tetrahedral unit than in the Al octahedral unit. These shorter and stronger bonds, when stretched, give rise to the characteristic peak at 750 cm^{-1} described in Sec II. However, by adding the 4 or 6 bonds in each unit, the total BO for the octahedral unit has an average value of 1.08 compared to the total BO for the tetrahedral unit of 1.01. This indicates that the octahedron is still a stronger polyhedral unit in γ-Al_2O_3.

V. SPECTROSCOPIC PROPERTIES

The spectroscopic properties of γ-Al_2O_3 consists of two parts: (1) The interband optical transitions from valence band to conduction band, (2) The core-level transitions from Al 1s, O 1s (K edges) and Al 2p (L_3 edge) to the empty CB states. The VB optical properties of γ-Al_2O_3 were calculated in the form of the frequency-dependent complex dielectric function $\varepsilon(\hbar\omega)=\varepsilon_1(\hbar\omega)+i\varepsilon_2(\hbar\omega)$ and the energy-loss function $\mathrm{ELF}[(\hbar\omega)=-\mathrm{Im}[1/\varepsilon(\hbar\omega)]$. The interband optical calculations were performed in the standard one-electron approximation within the random-phase approximation using the electronic structures from the ground-state LDA calculation.[47] No special adjustment for the band gap was attempted and the calculation includes the full momentum matrix elements between VB and CB states using *ab initio* wave functions at 864 k points in the irreducible portion of the BZ. The calculated results are shown in Fig. 12. The

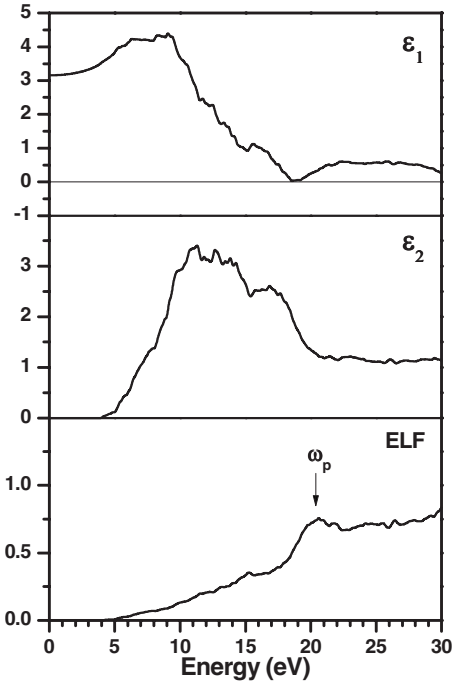

FIG. 12. The calculated valence-band optical spectra of γ-Al_2O_3: (a) $\varepsilon_1(\hbar\omega)$; (b) $\varepsilon_2(\hbar\omega)$; and (c) ELF$(\hbar\omega)$. The Plasmon frequency ω_p is indicated by the arrow.

calculated $\varepsilon_2(\hbar\omega)$ has a peak at 11 eV and a broad shoulder at about 16.7 eV. These features are comparable to the ones obtained by Ahujal *et al.*[29] using a different method and a slightly different structural model. The real part $\varepsilon_1(h\omega)$ was obtained from Kronig-Kramers conversion of the $\varepsilon_2(\hbar\omega)$. The optical dielectric constant $\varepsilon_1(0)$ has a value of 3.15. This value compares well with $\varepsilon_\infty=3.11$ using an entirely different method.[33] The square root of $\varepsilon_1(0)$ is frequently used to estimate the optical refractive index n. We obtained a value of $n=1.78$ for γ-Al_2O_3. Unfortunately, we cannot locate any experimentally measured refractive index data to compare with. The values of $\varepsilon_1(0)$ and n for α-Al_2O_3 in similar calculations are 3.14 and 1.77, respectively.[78,79] The plasma frequency ω_p corresponds to the frequency of collective electron excitation in the bulk crystal. In the present calculation, ω_p was identified to be 20.5 eV from the peak position in the energy-loss spectra. It is obvious that this peak is not as prominent as one would like to see because of the limited accuracy of the optical-absorption spectrum at higher transition energies. The numerical inaccuracy in the high-frequency region is greatly amplified in the ELF$(\hbar\omega)$ which is inversely proportional to $\varepsilon(\hbar\omega)$.

The XANES absorption edges (O-*K*, Al-*K*, Al-L_3) of γ-Al_2O_3 are calculated using the supercell OLCAO method which takes the core-hole interaction into account.[80] This method has emerged as one of the most accurate methods for XANES/ELNES spectral calculation for inorganic crystals in recent years. It has been successfully applied to a large number of complex crystals and their interfaces, surfaces, grain boundaries, and other microstructures.[45,73,81–95] Since the method of such calculations has been described in many recent papers, we only outline the calculations briefly here. A $2\times2\times1$ supercell (160 atoms) for γ-Al_2O_3 was used in the calculation. Because all atoms in the present model of γ-Al_2O_3 are nonequivalent, the spectra were calculated for each of the 16 Al ions (*K* and L_3 edges) and 24 O ions (O-*K* edge) in the unit cell. For each target atom, the calculation entails separate evaluations for the initial state (the core state in the ground-state calculation) and the final states (the conduction-band states with one of the core electron promoted to the bottom of the conduction band).[80] The final spectrum is obtained as the transition probability from the initial to the final state in accordance with the Fermi Golden rule.[96] The dipole transition matrix elements between the initial and the final states are explicitly included using 8 *k* points in the reduced BZ of the supercell to ensure accuracy. The transition energy is obtained as the difference in the total energies between the initial and the final-state calculations of the supercell for each spectrum.

Figure 13 shows the calculated Al-*K*, Al-L_3, and O-*K* edges for γ-Al_2O_3. For Al, the total edge is the weighted sum of the spectra of Al_{tet} and Al_{oct} which are also presented. Likewise, the total spectrum for O-*K* edge is the weighted sum of those of $O_{3\text{-fold}}$ and $O_{4\text{-fold}}$. As has been pointed out in numerous cases,[45,81,86,90,94,95] the spectral features including the absorption edge on set, depend sensitively on the local bonding environment of each cation or anion. It is impossible to experimentally distinguish the spectra from the two types of Al ions and two types of O ions in the actual measurement. This has contributed to difficulties in the interpretation of the measured XANES data. Even for ions with the same local bonding environment say, Al_{tet}, their spectra can be somewhat different from each other because these atoms are not equivalent. So, the spectra shown in Fig. 13 are the averaged spectra of the 6 (10) for Al_{tet} (Al_{oct}) and 12 (12) for $O_{3\text{-fold}}$ ($O_{4\text{-fold}}$) calculations. It is clear that the combined total spectra are fundamentally different from their constitutive groups. A more detailed inspection reveals that even within each group of ions with similar local bonding, their edge spectra can vary depending on the structural details such as bond lengths and bond angles. This fact has been amply demonstrated in a recent comprehensive study of ten inorganic crystals within the Y-Si-O-N series.[36] The calculated Al-*K*, Al-L_3, and O-*K* edges in γ-Al_2O_3 are noticeably different from those in α-Al_2O_3 which has unique octahedrally bonded Al and fourfold bonded O sites.[80]

There are only a few published papers with experimentally measured ELNES/XANES spectra for γ-Al_2O_3.[15–17] These are shown in Fig. 14 for Al-*L* and in Fig. 15 for O-*K* together with the calculated spectra. The overall agreement between the calculated and the measured spectra is very satisfactory. The main discrepancy in the Al-*L* edge appears to be in the relative intensities of the double peak above the edge on set. Kimoto *et al.*[17] attributed these two peaks, which are separated by about 1.6 eV, to Al_{tet} and Al_{oct} on the basis of a similar calculation using the structure of the η phase. The present results that are obtained by using the correct structural model for γ-Al_2O_3 show that these two peaks mainly come from the Al_{tet} site. The mixing with Al_{oct} only modifies the peak intensity and makes them less sharp. It is also noted that the peak positions and the edge on-sets in the Al-*L* edge from the three different experimental groups are slightly different. This could be attributed to variations in

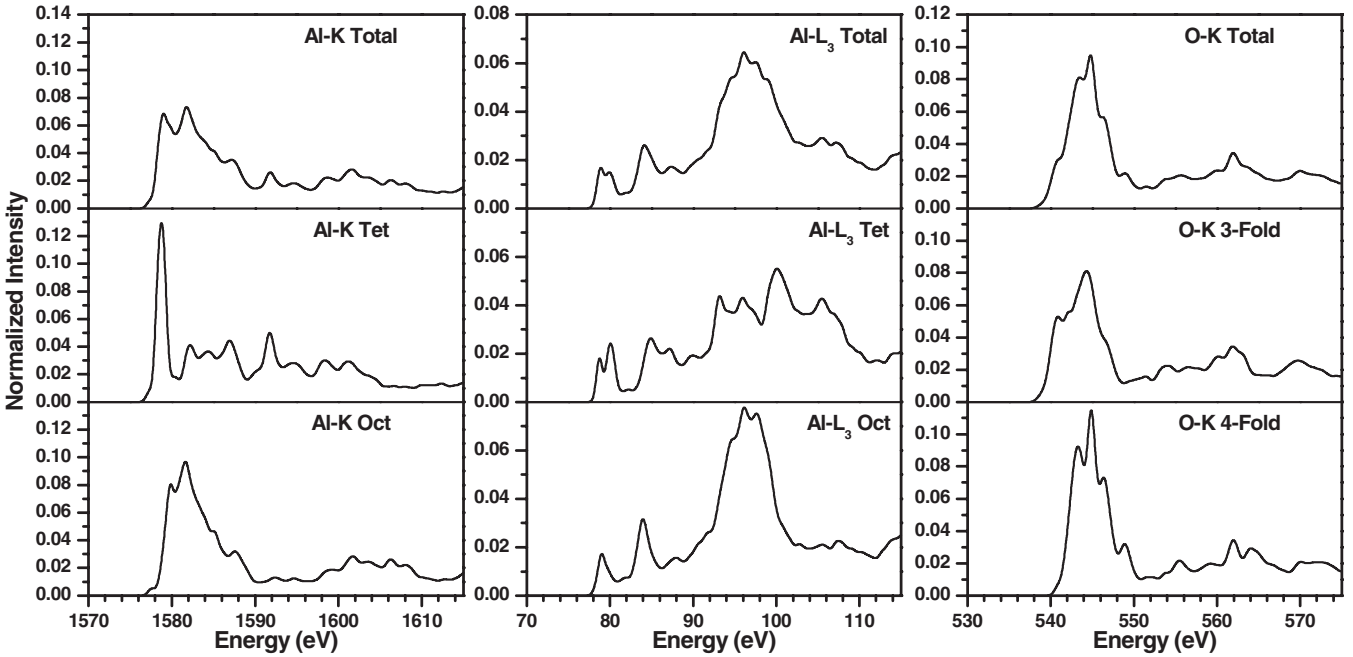

FIG. 13. Calculated XANES spectra for γ-Al_2O_3: (a) Al-K edge; (b) Al-L_3 edge; (c) O-K edge. The top panel is for the total spectrum which is the sum of spectra for all the atoms of the type. The lower panels are the edge spectra from atoms with different local coordination.

the samples used in the measurements. The minor disagreement in the Al-L edges with experiment can also be explained by the possible surface effect where the surface Al atoms are fivefold bonded.[18] This could change the intensity ratio of the two leading peaks in the measured spectrum. Calculations of the XANES spectra for other transition alumina[97] show that the Al-L edge and the O-K edge differ from those of γ-Al_2O_3 even when their local coordination is the similar. In Fig. 15, the experimental data for the O-K edge[15] are presented for comparison. As can be seen, the agreement in the asymmetric shape of the spectrum with the calculation is very satisfactory. The experimental spectrum has much less energy resolution so some of the features present in the calculated spectrum cannot be resolved.

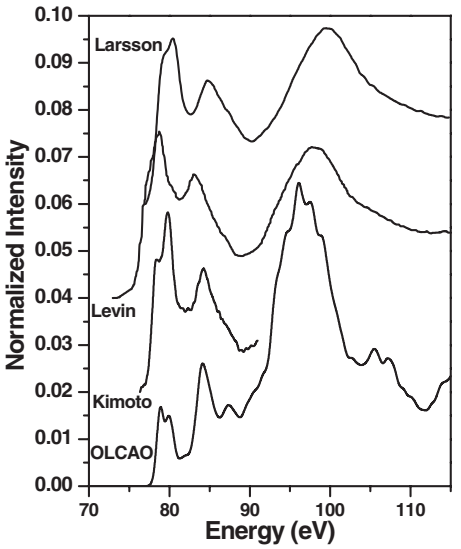

FIG. 14. Comparison of the calculated Al-L_3 edge in γ-Al_2O_3 with three sets of experiments. (Larson: Ref. 16; Levin, Ref. 15; and Kimoto, Ref. 17.)

VI. DISCUSSION AND SUMMARY

The above rather comprehensive list of the calculated physical properties of γ-Al_2O_3 based on the proposed structure in Ref. 30 and their good agreement with the available experimental data give credence to this structure for γ-Al_2O_3. In the cases where the agreement is less than desirable, it can be attributed to possible sample variations since γ-Al_2O_3 is not in the form of a single crystal and may not even be totally stoichiometric. Various previous studies indicated the importance of the surface effect in porous γ-Al_2O_3. The present calculation is for a bulk γ-Al_2O_3 model with a unit cell with 40 atoms. When performing a comparison with the measured physical properties, this fact must be taken into consideration.

Our main conclusions are that γ-Al_2O_3 should "not" be considered to have an underlying crystalline structure (cubic

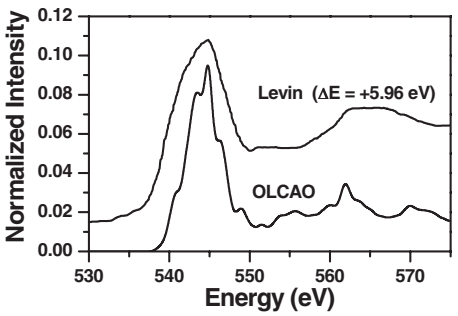

FIG. 15. Comparison of the calculated O-K edge in γ-Al_2O_3 with the measurement from Ref. 15. The experimental curve is shifted by 5.96 eV to align the main peak with the calculation.

TABLE IV. Percentage of Al_{tet}, Al_{oct}, $O_{3\text{-fold}}$, $O_{4\text{-fold}}$ sites in Alumina phases.

Crystal	$\%Al_{tet}$	$\%Al_{oct}$	$Al_{tet}:Al_{oct}$	$\%O_{3\text{-fold}}$	$\%O_{4\text{-fold}}$	$O_{3\text{-fold}}:O_{4\text{-fold}}$
α-Al_2O_3	0	100	0	0	0	-
γ-Al_2O_3	37.5	62.5	0.60	50	50	1
θ-Al_2O_3	50	50	1	66.7	33.3	2
κ-Al_2O_3	25	75	0.333	66.7	33.3	2
spinel	33.3	66.7	0.5	0	100	0

spinel or otherwise) accompanied by defects (cation vacancies). Rather, it should be viewed as an amorphous random network structure of Al–O bonds where Al can be either tetrahedrally or octahedrally bonded, and the corresponding O will have to be either threefold or fourfold bonded. In such a structure, the notion of cation vacancy in a regular spinel lattice loses its meaning entirely. Indeed, a detailed simulation studies by Wolverton *et al.*,[25] Krokidis *et al.*,[34] Digne *et al.*[35] and Paglia *et al.*[28] already show that the nonspinel model where no spinel sites are occupied by Al atoms is the best representative for the structure of γ-Al_2O_3. The calculated electronic structure of γ-Al_2O_3 has significant differences when compared to α-Al_2O_3 and θ-Al_2O_3(Ref. 40) calculated using the same method. This is mainly due to different percentages of Al_{tet}, Al_{oct}, $O_{3\text{-fold}}$, and $O_{4\text{-fold}}$. Table IV lists the percentages of these local units for α-Al_2O_3, γ-Al_2O_3, and the other two transition alumina θ-Al_2O_3(Refs. 6 and 40) and κ-Al_2O_3.[6] Hence, an appropriate model for γ-Al_2O_3 probably should be that of a glasslike random network structure with well defined local short-range order but no long-range order. Additional modeling work in this direction is highly desirable. The structure determined by Ref. 30 clearly represents the smallest unit cell for an amorphous network that accounts for all the essential characteristics of γ-Al_2O_3. It is highly desirable to extend the modeling effort to larger amorphous models for γ-Al_2O_3 and even those with internal voids and surfaces which can rationalize the difference with some experimental observations. In these amorphouslike models, there could be some variations in the percentages of Al_{tet} and Al_{oct} as well as $O_{3\text{-fold}}$ and $O_{4\text{-fold}}$.

The above viewpoint is further supported by several facts. First, there exist highly localized states at the top of the VB, characteristic of an amorphous solid. Second, the variations in the Mulliken effective charges and BO values in the present model also indicate that the atomic structure within the 40-atom cell is quite disordered. This is true for both the cations and the anions and within groups of atoms with the same type of local bonding. Third, the calculation of the mode-Grüneisen parameter shows two negative values, pointing to the fact that γ-Al_2O_3 is amorphouslike. Fourth, the calculated vibrational DOS show broadened features characteristic of an amorphous solid. Lastly, the comparison between the calculated and measured XANES spectra supports this view. The individual XANES/ELNES spectra of atoms with the same type of bonding environment also show variations yet the sum of these spectra show agreement with experiments. Although there are some minor discrepancies in the comparison related to the relative peak strengths, they are explained by the experimental samples which may not correspond exactly to the pure stoichiometric γ-Al_2O_3. Indeed, molecular dynamic simulations[41] on amorphous Al_2O_3 indicated that the structure of amorphous Al_2O_3 has a close resemblance to γ-Al_2O_3 surfaces with different coordinating units including fivefold Al at different densities.

The calculation of the phonon spectrum in the present model of γ-Al_2O_3 is particularly challenging since there is no internal symmetry in the model to reduce the calculation. Furthermore, the calculation of the temperature-dependent Gibb's free energy $G(P,T)$ in γ-Al_2O_3 points to the eventual description of the various phases in transition alumina based on a full thermodynamic treatment. The calculation of bulk elastic properties indicates that γ-Al_2O_3 is less rigid than α-Al_2O_3. The model used here does not include any porosity at all. If the porous nature of γ-Al_2O_3 is taken into account, the mechanical properties will likely be even weaker. Such studies will be important for future large scale modeling of γ-Al_2O_3.

ACKNOWLEDGMENTS

This work was supported by the U.S. Department of Energy under Grant No. DE-FG02-84DR45170. This research used the resources of NERSC supported by the Office of Science of DOE under Contract No. DE-AC03-76SF00098.

*Corresponding author: chingw@umkc.edu

[1] E. Dörre and H. Hübner, *Alumina* (Springer-Verlag, Berlin, 1984).
[2] A. Bell, Science **299**, 1688 (2003).
[3] Science of Alumina, topical issue of J. Am. Ceram. Soc. **77** (2), (1994).
[4] Alumina, topical issue of J. Am. Ceram. Soc. **86** (4), (2003).
[5] K. Wefers and C. Misra, *Oxides and Hydroxides of Aluminium*, (Alcoa Laboratory, Pittsburgh, 1987), Technical Paper No. 19.
[6] R.-S. Zhou and R. L. Snyder, Acta Crystallogr., Sect. B: Struct. Sci. **47**, 617 (1991).
[7] F. Robinson and M. Gillet, Thin Solid Films **98**, 179 (1982).
[8] Z. Xu, F.-S. Xiao, S. K. Purnell, O. Alexeev, S. Kawi, S. E. Deutsch, and B. C. Gates, Nature (London) **372**, 346 (1994).

[9] V. S. Y. Lin, J. Am. Ceram. Soc. **124**, 9040 (2002).
[10] M. Trueba and S. P. Trasatti, Eur. J. Inorg. Chem. **2005**, 3393.
[11] T. Taniike, M. Tada, Y. Morikawa, T. Sasaki, and Y. Iwasawa, J. Phys. Chem. B **110**, 4929 (2006).
[12] P. Euzen, P. Raybaud, X. Krokidis, H. Toulhoat, J.-L. Le Loarer, J.-P. Jolivet, and C. Froidefond, in *Handbook of Porous Materials*, edited by F. Schüth, K. Sing, and C. Weitkamp (Wiley, Weinheim, 2002), Vol. 3. Chap. 4.7.2, pp. 1591–1677.
[13] M. Kefi, P. Jonnard, F. Vergand, C. Bonnelle, and E. Gillet, J. Phys.: Condens. Matter **5**, 8629 (1993).
[14] J. Y. Ying, J. B. Benziger, and H. Gleiter, Phys. Rev. B **48**, 1830 (1993).
[15] I. Levin, W. D. Kaplan, D. G. Bradon, H. Mullenjans, and M. Ruhle, Mater. Sci. Forum **207-209**, 749 (1996).
[16] A. Larson, J. Zackrisson, M. Halvarsson, and S. Ruppi, Inst. Phys. Conf. Ser. **165**, Symposium 6, 235 (2000).
[17] K. Kimoto, Y. Matsui, T. Nabatame, T. Yasuda, T. Mizoguichi, I. Tanaka, and A. Toriumi, Appl. Phys. Lett. **83**, 4306 (2003).
[18] S. Wang, A. Y. Borisevich, S. N. Rashkeev, M. V. Glazoff, K. Sohlberg, S. J. Pennycook, and S. T. Pantelides, Nat. Mater. **3**, 143 (2004).
[19] B. Ealet, M. H. Elyakhloufi, E. Gillet, and M. Ricci, Thin Solid Films **250**, 92 (1994).
[20] C. Pecharroman, I. Sobrados, J. E. Iglesias, T. Gonzales-Carreno, and J. Sanz, J. Phys. Chem. B **103**, 6160 (1999).
[21] C. S. John, N. C. M. Alma, and G. R. Hays, Appl. Catal. **6**, 341 (1983).
[22] Shang-Di Mo, Yong-Nian Xu, and W. Y. Ching, J. Am. Ceram. Soc. **80**, 1193 (1997).
[23] M.-H. Lee, C.-F. Cheng, V. Heine, and J. Klinowski, Chem. Phys. Lett. **265**, 673 (1997).
[24] F. H. Streitz and J. W. Mintmire, Phys. Rev. B **60**, 773 (1999).
[25] C. Wolverton and K. C. Hass, Phys. Rev. B **63**, 024102 (2000).
[26] G. Gutierrez, A. Taga, and B. Johansson, Phys. Rev. B **65**, 012101 (2001).
[27] C. M. Fang, R. Metselaar, H. T. Hintzen, and G. de With, J. Am. Ceram. Soc. **84**, 2633 (2001).
[28] G. Paglia, C. E. Buckley, A. L. Rohl, B. A. Hunter, R. D. Hart, J. V. Hanna, and L. T. Byrne, Phys. Rev. B **68**, 144110 (2003).
[29] R. Ahuja, J. M. Osorio-Guillenl, J. S. de Almeidal, B. Holml, W. Y. Ching, and B. Johansson, J. Phys.: Condens. Matter **16**, 2891 (2004).
[30] E. Menendez-Proupin and G. Gutierrez, Phys. Rev. B **72**, 035116 (2005).
[31] H. P. Pinto, R. M. Nieminen, and S. D. Elliot, Phys. Rev. B **70**, 125402 (2004).
[32] G. Paglia, A. L. Rohl, C. E. Buckley, and J. D. Gale, Phys. Rev. B **71**, 224115 (2005).
[33] C.-K. Lee, E. Cho, H.-S. Lee, K. S. Seol, and S. Han, Phys. Rev. B **76**, 245110 (2007).
[34] X. Krokidis, P. Raybaud, A.-E. Gobichon, B. Rebours, P. Euzen, and H. Toulhoat, J. Phys. Chem. B **105**, 5121 (2001).
[35] M. Digne, P. Sautet, P. Raybaud, P. Euzen, and H. Toulhoat, J. Catal. **226**, 54 (2004).
[36] M. Sun, A. E. Nelson, and J. Adjaye, J. Phys. Chem. B **110**, 2310 (2006).
[37] I. Levin and D. Brandon, J. Am. Ceram. Soc. **81**, 1995 (1998).
[38] M. Digne, P. Raybaud, P. Sautet, B. Rebours, and H. Toulhoat, J. Phys. Chem. B **110**, 20719 (2006).
[39] G. Paglia, C. E. Buckley, and A. L. Rohl, J. Phys. Chem. B **110**, 20721 (2006).
[40] Shang-Di Mo and W. Y. Ching, Phys. Rev. B **57**, 15219 (1998).
[41] G. Gutierrez and B. Johansson, Phys. Rev. B **65**, 104202 (2002).
[42] G. Kresse and J. Hafner, Phys. Rev. B **47**, 558 (1993); J. Phys.: Condens. Matter **6**, 8245 (1994).
[43] G. Kresse and J. Furthmuller, Comput. Mater. Sci. **6**, 15 (1996).
[44] W. Y. Ching, J. Am. Ceram. Soc. **87**, 1996 (2004).
[45] W. Y. Ching, and P. Rulis, Phys. Rev. B **77**, 035125 (2008).
[46] Z. Lodziana and K. Parlinski, Phys. Rev. B **67**, 174106 (2003).
[47] W. Y. Ching, J. Am. Ceram. Soc. **73**, 3135 (1990).
[48] S. Baroni, S. de Gironcoli, A. D. Corso, and P. Giannozzi, Rev. Mod. Phys. **73**, 515 (2001).
[49] D. M. Ceperley and B. J. Alder, Phys. Rev. Lett. **45**, 566 (1980).
[50] J. Paier, R. Hirschl, M. Marsman, and G. Kresse, J. Chem. Phys. **122**, 234102 (2005).
[51] J. Xu, E. Huang, J. Lin, and L. Y. Xu, Am. Mineral. **80**, 1157 (1995).
[52] Ru Ju Wang, Wei Hua Wang, Feng Ying Li, Li Min Wang, Yong Zhang, Ping Wen, and Ji Fang Wang, J. Phys.: Condens. Matter **15**, 603 (2003).
[53] Jaroslav Fabian and Philip B. Allen, Phys. Rev. Lett. **79**, 1885 (1997).
[54] M. B. Kruger, Q. Williams, and R. Jeanloz, J. Chem. Phys. **91**, 5910 (1989).
[55] J. B. Wachtman, Jr., T. G. Scuderi, and G. W. Cleek, J. Am. Ceram. Soc. **45**, 319 (1962); *CRC Handbook of Chemistry and Physics*, 87th ed., edited by David R. Lide (Taylor & Francis, LLC, 2006); P. Richet, J. Xu, and H. K. Mao, Phys. Chem. Miner. **16**, 207 (1988); D. Gerlich, J. Phys. Chem. Solids **31**, 1188 (1970).
[56] Hongzhi Yao, L. Ouyang, and W. Y. Ching, J. Am. Ceram. Soc. **90**, 3194 (2007).
[57] *Statics of Deformable Solids*, edited by R. L. Bisplinghoff, J. W. Mar, and T. H. H. Pain (Dover, New York, 2002).
[58] W. Voigt, *Lehrbuch der Kristallphysik* (Teubner, Leipzig, 1928), pp. 716–761.
[59] A. Reuss, Z. Angew. Math. Mech. **9**, 49 (1929).
[60] R. Hill, Proc. Phys. Soc., London, Sect. A **65**, 349 (1952).
[61] Robert E. Newnham, *Properties of Materials, Anisotropy, Symmetry, Structure* (Oxford University Press, Oxford, 2005).
[62] W. Y. Ching, S.-D. Mo, I. Tanaka, and M. Yoshiya, Phys. Rev. B **63**, 064102 (2001).
[63] W. Y. Ching, S.-D. Mo, L. Ouyang, P. Rulis, I. Tanaka, and M. Yoshiya, J. Am. Ceram. Soc. **85**, 75 (2002).
[64] Lizhi Ouyang, Yong-Nian Xu, and W. Y. Ching, Phys. Rev. B **65**, 113110 (2002).
[65] Lzhi Ouyang and W. Y. Ching, Appl. Phys. Lett. **81**, 229 (2002).
[66] W. Y. Ching, Yong-Nian Xu, and L. Ouyang, Phys. Rev. B **66**, 235106 (2002).
[67] W. Wong-Ng, W. Y. Ching, Y.-N. Xu, J. A. Kaduk, I. Shirotani, and L. Swartzendruber, Phys. Rev. B **67**, 144523 (2003).
[68] W. Y. Ching, L. Ouyang, and Yong-Nian Xu, Phys. Rev. B **67**, 245108 (2003).
[69] Yong-Nian Xu, W. Y. Ching, and Y. Chiang, J. Appl. Phys. **95**, 6583 (2004).
[70] W. Y. Ching, L. Ouyang, Hongzhi Yao, and Y.-N. Xu, Phys. Rev. B **70**, 085105 (2004).
[71] P. Rulis, L. Ouyang, and W. Y. Ching, Phys. Rev. B **70**, 155104 (2004).
[72] W. Y. Ching, P. Rulis, Yong-Nian Xu, and L. Ouyang, Mater. Sci.

Eng., A **422**, 147 (2006).
[73] P. Rulis, Hongzhi Yao, L. Ouyang, and W. Y. Ching, Phys. Rev. B **76**, 245410 (2007).
[74] W. Y. Ching, G.-L. Zhao, and Yi He, Phys. Rev. B **42**, 10878 (1990).
[75] M.-Z. Huang and W. Y. Ching, Phys. Rev. B **54**, 5299 (1996).
[76] Ming-Zhu Huang, Lizhi Ouyang, and W. Y. Ching, Phys. Rev. B **59**, 3540 (1999).
[77] R. S. Mullikan, J. Am. Chem. Soc. **23**, 1833 (1955); **23**, 1841 (1955).
[78] W. Y. Ching (unpublished).
[79] Y.-N. Xu and W. Y. Ching, Phys. Rev. B **43**, 4461 (1991).
[80] Shang-Di Mo and W. Y. Ching, Phys. Rev. B **62**, 7901 (2000).
[81] I. Tanaka, T. Mizoguchi, T. Sekine, H. He, K. Kimoto, S.-D. Mo, and W. Y. Ching, Appl. Phys. Lett. **78**, 2134 (2001).
[82] Shang-Di Mo, and W. Y. Ching, Appl. Phys. Lett. **78**, 3809 (2001).
[83] W. Y. Ching, Shang-Di Mo, and Yu Chen, J. Am. Ceram. Soc. **85**, 11 (2002).
[84] Y.-N. Xu, Yu Chen, Shang-Di Mo, and W. Y. Ching, Phys. Rev. B **65**, 235105 (2002).
[85] Y. Chen, S. D. Mo, M. Kohyama, H. Kohno, S. Takeda, and W. Y. Ching, Mater. Trans. **43**, 1430 (2002).
[86] I. Tanaka, T. Mizoguchi, M. Matsui, S. Yoshioka, F. Oba, H. Adachi, T. Okajima, M. Umesaki, W. Y. Ching, Y. Inoue, M. Mizuno, and Y. Shirai, Nat. Mater. **2**, 541 (2003).
[87] P. Rulis, W. Y. Ching, and M. Kohyama, Acta Mater. **52**, 3009 (2004).
[88] T. Mizoguchi, I. Tanaka, S. Yoshioka, M. Kunisu, T. Yamamoto, and W. Y. Ching, Phys. Rev. B **70**, 045103 (2004).
[89] W. Y. Ching, L. Ouyang, P. Rulis, and I. Tanaka, Phys. Status Solidi B **242**, R94 (2005).
[90] T. Mizoguchi, Y. Sato, J. P. Buban, K. Matsunaga, T. Yamamoto, and Y. Ikuhara, Appl. Phys. Lett. **87**, 241920 (2005).
[91] W. Y. Ching and Paul Rulis, Phys. Rev. B **73**, 045202 (2006).
[92] T. Mizoguchi, T. Sasaki, S. Tanaka, K. Matsunaga, T. Yamamoto, M. Kohyama, and Y. Ikuhara, Phys. Rev. B **74**, 235408 (2006).
[93] T. Mizoguchi, A. Seko, M. Yoshiya, H. Yoshida, W. Y. Ching, and I. Tanaka, Phys. Rev. B **76**, 195125 (2007).
[94] S. Aryal, P. Rulis, and W. Y. Ching, Am. Mineral. **93**, 114 (2008).
[95] W. Y. Ching and P. Rulis, Phys. Rev. B **77**, 125116 (2008).
[96] R. F. Egerton, *Electron-Energy Loss Spectroscopy in the Electron Microscope* (Plenum, New York, 1996), Chap. 5.
[97] W. Y. Ching (unpublished).